PHYSICAL REVIEW B VOLUME 18, NUMBER 10 15 NOVEMBER, 1978

Two-band model for $NbSe_3$ (Ohmic regime)

N. P. Ong
Department of Physics, University of Southern California, Los Angeles, California 90007
(Received 10 July 1978)

The charge-density-wave (CDW) linear-chain metal $NbSe_3$ shows striking non-Ohmic behavior when the applied electric field exceeds ~ 0.1 V/cm. Hall effect, transverse magnetoresistance, conductivity anisotropy, and Shubnikov–de Haas measurements using sufficiently low current densities to avoid Ohmic breakdown have been published. We propose a simple two-band model to account for the temperature dependence of these quantities as well as the (magnetic) field dependence of the Hall constant in the Ohmic regime below 58 K. The model has six unknowns (carrier concentrations and mobilities) that are fixed by six experimental numbers at each temperature T. The solution shows that all the mobilities obey a power-law behavior versus T, whereas the carrier concentrations are both T independent up to 40 K. Above 40 K the hole population rises sharply, analogous to the theoretical predictions for an excitonic insulator. This implies that the CDW gap occurs on the hole surface. Using the parameters of the model, we have recomputed the resistivities, Hall constant, and magnetoresistance, and they have been shown to agree with all the available experimental data. Thus the conventional single-particle picture with the additional hypothesis of a BCS-type gap on the hole surface is adequate for understanding the transport properties of $NbSe_3$ in the zero-frequency-Ohmic regime. We also interpret the SdH data in terms of the two-band model.

I. INTRODUCTION

Below the transition temperature T_1 (~142 K) the transport properties of the charge-density-wave (CDW) metal[1] $NbSe_3$ are conveniently divided into three regimes for the purpose of analysis. These are, (i) the zero-frequency low-current (Ohmic) regime; (ii) the zero-frequency high-current (non-Ohmic) regime; (iii) the high-frequency (above ~100 MHz) low-current regime. (There clearly exists a fourth regime: the high-frequency non-Ohmic regime, but no experimental data exist in this regime.) Strong interest has been generated by the study of regimes (ii) and (iii) because of the possibility of studying experimentally the dynamics of a sliding CDW in a real metal. Such studies will shed light on (a) the nonlinear dynamics associated with a drifting CDW,[2] (b) the nature of the pinning forces impeding its motion, and (c) the feasibility of realizing a system in which the sliding Fröhlich mode leads to superconductivity. With regard to (b) the ease with which the pure compound is alloyed[3] or intercalated[4,5] with Li makes it an attractive system in which to study the pinning effects of the CDW condensate due to impurities. Such impurity studies are presently underway and show[3] that the behavior in regimes (ii) and (iii) are exceedingly sensitive to impurity concentrations.

Most of the galvanomagnetic[1,6] as well as Fermiology[7-9] studies done to date have been in regime (i) where the applied electric fields are sufficiently low to avoid Ohmic breakdown. Although regime (i) is of less interest as compared to (ii) and (iii) it is essential to obtain a picture of the "normal" regime that is as complete as experimentally feasible so that the intriguing additional effects (conductivity enhancement) in regimes (ii) and (iii) can be isolated and analyzed. In this paper we construct a simple two-band model that will account for the galvanomagnetic and conductivity anisotropy data [regime (i)] presented in Refs. 1, 6, and 8. Single crystals of $NbSe_3$ usually grow in the shape of long ribbons with the long side along the (chain) b axis and the wider transverse dimension along the c axis. Low-magnetic-field Hall measurements with $\boldsymbol{H}$ along a^* have been reported by Ong and Monceau (OM).[6] High-field-Hall measurements in the same geometry have been presented by Fleming, Polo, and Coleman (FPC).[8] Transverse magnetoresistance ($H||a^*$) were presented in the preceding paper[1] as well as conductivity anisotropy measurements. In addition, extensive Shubnikov–de Haas (SdH) measurements have been carried out by Monceau (M),[7] Fleming *et al.* (FPC)[8], and Monceau and Briggs (MB).[9] It will be seen that a two-band model can satisfactorily account for much of the data in these studies below the T_2 transition. Out of this analysis we obtain the temperature dependence of the four mobilities in the b-c plane as well as the carrier concentration in both bands. In support of the conventional CDW model,[10,11] our analysis shows that the carrier concentrations are temperature independent below ~40 K. Above 40 K the hole population rises dramatically in analogy with the increase in thermally excited quasiparticles across the Fermi surface (FS) gap of an excitonic insulator.[12] In contrast the electron population remains con-

stant up to 58 K. Persuasive evidence identifies the electron pocket with the ellipsoidal pocket seen in the SdH oscillations of M, FPC, and MB. The evidence for a hole pocket is unclear at present. This two-band analysis enables us to disentangle the individual contributions of the four mobilities to the conductivity anisotropy, the Hall signal and the transverse magnetoresistance. It will be shown for instance that the twelve-fold increase[6] in $|R_H(0)|$ at T_2 is compatible with the twofold rise in the longitudinal resistivity and the still smaller rise in the transverse resistivity. The zero crossing of $R_H(0)$ at ~15 K is due to the faster increase of the hole mobilities relative to the electron mobilities as the temperature drops, and not to any change in the carrier population. On the other hand, the giant anomaly in the resistivities is due to the rapid change in hole concentration between ~40 K and T_2. No anomalous structure is reflected in any of the mobilities. This is also presumably the case at the upper transition, although the lack of sufficient galvanomagnetic data and theoretical considerations preclude the extension of our analysis beyond 58 K.

II. TWO-BAND MODEL

The single-particle picture with a semiclassical treatment of the transport properties[13] has been remarkably successful when applied to ordinary metals and semiconductors. To make the analysis manageable we have assumed the simplest Boltzmann equation-relaxation time approach in computing the galvanomagnetic response. Since the details are found in many text books[14] we will present results only. The assumptions intrinsic to the model are as follows. (a) At low-temperatures there exist two closed FS pockets containing electrons and holes, respectively. (b) These pockets are ellipsoids with their principal axes along a^*, b, and c. (c) The relaxation time is assumed isotropic and independent of magnetic field and complications such as intense scattering from "hot spots" on the FS will be disregarded. Assumptions (a) and (b) are indicated by the SdH data which show two branches. The prominent branch is consistent with an ellipsoid of moderate anisotropy with principal axes along a^*, b, and c. Less conclusive evidence is available for the other pocket which we take to be ellipsoidal as well. The third assumption will be discussed together with the computed magnetoresistance. No further justification of the assumptions will be discussed except to appeal to the comparison of the computations with the experiments.

In the Boltzmann equation approach the current is given by[14]

$$\vec{J}=\sum_{\vec{k}}\left(-\frac{\partial f}{\partial\epsilon}\right)e^2\tau\vec{v}_{\vec{k}}\cdot\vec{A}\vec{v}_k=\frac{2e^2\tau}{(2\pi)^3}\int_{\epsilon_F}\frac{dS_F}{|\hbar v_{\vec{k}}|}\vec{v}_{\vec{k}}\cdot\vec{A}\vec{v}_{\vec{k}}\,, \tag{1}$$

$$\vec{A}\equiv\left(\vec{E}-\frac{e\tau}{(m_1m_2)^{1/2}}\vec{H}\times\vec{E}\right)\Big/\left(1+\frac{e^2\tau^2}{m_1m_2}H^2\right), \tag{2}$$

where $\vec{v}_{\vec{k}}=\hbar^{-1}\partial\epsilon_{\vec{k}}/\partial\vec{k}$ is the velocity of the carrier at $\vec{k}$, f is the Fermi-dirac distribution, τ the isotropic relaxation time, m_i the effective mass along the i axis and the integral in (1) is over the FS. In general the relaxation time may be anisotropic as well, aspecially if the system is highly anisotropic. However, the galvanomagnetic measurements analyzed here cannot distinguish between mass and relaxation time anisotropy. In the spirit of the model we will describe all the observed anisotropy in terms of the mobilities. Assuming a quadratic dispersion it is straightforward to reduce Eq. (1) to the familiar conductivity matrix for electrons (with $\vec{H}$ along the three axis)

$$\vec{\sigma}_n=\frac{ne}{[1+(\mu_1\mu_2H)^2]}\begin{pmatrix}\mu_1 & -\mu_1\mu_2H\\ \mu_1\mu_2H & \mu_2\end{pmatrix}, \tag{3}$$

where the mobility $\mu_i\equiv e\tau/m_i$ has been introduced and n the carrier concentration is given by

$$n=\frac{2}{(2\pi)^3}\int_0^{\epsilon_F}d\epsilon\int_\epsilon\frac{dS_F}{|\hbar v|}\,. \tag{4}$$

Calling the hole concentration p and the hole mobilities ν_i we have for the total conductivity matrix

$$\vec{\sigma}=\frac{n}{[1+(\mu_1\mu_2H)^2]}\begin{pmatrix}\mu_1 & -\mu_1\mu_2H\\ \mu_1\mu_2H & \mu_2\end{pmatrix}+\frac{p}{[1+(\nu_1\nu_2H)^2]}\begin{pmatrix}\nu_1 & +\nu_1\nu_2H\\ -\nu_1\nu_2H & \nu_2\end{pmatrix}. \tag{5}$$

For convenience we have absorbed e into n and p. All quantities in Eq. (5) are assumed positive. The sign difference in the off-diagonal elements has been shown explicitly. In the experimental situation[15,16] it is actually the resistivity matrix $\vec{\rho}=\vec{\sigma}^{-1}$ which is measured. Explicitly, if the constant current is along the two-axis (b axis) and the magnetic field along the three-axis (a^* axis) the electric field along the one and two axes is given by $\vec{E}=\vec{\rho}\cdot\vec{J}$ where $\vec{J}=(0,J_0)$. The Hall voltage is proportional to $E_1=\rho_{12}J_0$ whereas the transverse magnetoresistance is measured by $E_2=\rho_{22}J_0$. Inverting the matrix in Eq. (5) we may show that the Hall constant $R_H\equiv E_1/(HJ_0)$ is given by

$$R_H(H)=-A(H)/(B_1B_2+A^2H^2)\,, \tag{6}$$

where

$$A(H)\equiv n\mu_1\mu_2/[1+(\mu_1\mu_2H)^2]-p\nu_1\nu_2/[1+(\nu_1\nu_2H)^2] \tag{7}$$

and

$$B_i \equiv n\mu_i/[1+(\mu_1\mu_2 H)^2] + p\nu_i/[1+(\nu_1\nu_2 H)^2]. \quad (8)$$

In the limits of zero field and infinite field Eq. (6) reduces to

$$R_0 \equiv R_H(0) = -(n\mu_1\mu_2 - p\nu_1\nu_2)/(n\mu_1 + p\nu_1)(n\mu_2 + p\nu_2) \quad (9)$$

and

$$R^\infty \equiv R_H(\infty) = -1/(n-p). \quad (10)$$

We have adopted the convention that R_H is negative if there are no holes present ($p=0$). From Eqs. (9) and (10) it is clear that whereas the sign of R^∞ is determined by the more populous carrier type the sign of R_H at low fields is also influenced by the relative sizes of the mobilities and the anisotropy in each band. The longitudinal resistance in the presence of a weak magnetic field behaves as $\rho(H) = \rho_0(1+\mu_M^2 H^2)$ where μ_M is the effective magnetoresistance mobility. From the diagonal element of the resistivity matrix we calculate

$$\mu_M^2 = \frac{\rho_{22}(H) - \rho_{22}(0)}{H^2} = \frac{np\mu_1\nu_1(\mu_2+\nu_2)^2}{(n\mu_1+p\nu_1)(n\mu_2+p\nu_2)}. \quad (11)$$

We note that μ_M vanishes if either n or p is zero. This is the expected result in a single band where the relaxation time is energy independent. The Hall field prevents any deflection of the carriers and the measured longitudinal resistance is unaffected by a transverse magnetic field. Furthermore μ_M vanishes if $\mu_2 = -\nu_2$, i.e., if the two bands have the same sign of charge and the same longitudinal mobility. The longitudinal mobility is responsible for this cancellation because the longitudinal velocity sets up the Lorentz force. As mentioned above the mobilities themselves are assumed to be field independent. In principle the relaxation time can have a field dependence such as $\tau^{-1} = \tau_0^{-1} + \alpha^2 H^2$. However, since the observed magnetoresistance at low temperatures is very large we shall assume that the dominant effect is due to the deflection of carrier trajectories arising from mutual (partial) cancellation of the Hall field of the holes and electrons. The existance of hot spots on the FS where electron-phonon interaction is enhanced can also affect the magnetoresistance. But in the low-field limit where the carriers sample only a limited portion of the FS before being scattered we may neglect such complications.

In the model described by Eq. (5) there are six unknowns, n, p, μ_1, ν_1, μ_2, and ν_2. At each temperature there are four measured quantities: the Hall constant $R_H(0)$, the transverse magnetoresistance, and the zero-field resistivities

$$\rho_i \equiv (n\mu_i + p\nu_1)^{-1}. \quad (12)$$

The Hall constant at infinite field R^∞ which can be measured only at very low temperatures provides a constraint through Eq. (10). Finally, the field dependence of R_H at each temperature provides the sixth equation to determine the six unknowns, leaving no adjustable parameters. Although the analytical inversion of the six equations is rather difficult the numerical solution may be readily accomplished by first forming the dimensionless constants

$$C_1 \equiv \mu_M(\rho_1\rho_2)^{1/2}/(R^\infty - R_0), \quad (13)$$

$$C_2 \equiv \mu_M(\rho_1\rho_2)^{1/2}/R^\infty. \quad (14)$$

(It turns out that C_1 and C_2 may be measured very accurately even if the sample dimensions are unknown. This is because $(\rho_1\rho_2)^{1/2}$ (determined by Montgomery's[17] technique) is independent[1] of b and c, and is linear in a (the dimension along $\vec{H}$). This is also true of $R_H(H)$. μ_M is independent of sample dimensions. Thus C_1 and C_2 are the ratio of voltmeter readings). A closed subset of three equations can be formed which expresses C_1, C_2, and $R_H(H)/R^\infty$ in terms of the three dimensionless parameters

$$r = n/p, \quad \eta = \mu_1/\nu_1, \quad \text{and } \xi = \mu_2/\nu_2. \quad (15)$$

Finally, these three equations can be solved numerically for r, ξ, and η. Details of the solution are presented in the appendix. We note that insofar as C_1, C_2, and R_H/R^∞ do not depend on sample dimensions the values r, η, and ξ will not be influenced by uncertainties in sample dimensions. However, to compute μ_1, ν_1, μ_2, and ν_2 separately we need to use the anisotropy ρ_1/ρ_2 which, of course, depends on the ratio b/c.

In the foregoing analysis we have assumed that the carrier concentrations are temperature dependent. This enables us to use the value of R^∞ measured at 2 K to fix the value of $(p-n)$. (It is not possible to measure R^∞ at elevated temperatures with currently available magnetic fields.) This assumption is justified in a self-consistent fashion by the solutions below 36 K which show that r in Eq. (15) is temperature independent. However, this assumption is invalid at temperatures above ~40 K where a previous analysis[18] of the non-Ohmic conductivity data shows that substantial thermal excitation of quasiparticles across the CDW gap occurs. This is also clearly demonstrated by Hall data in Figs. 3 and 4 of the previous paper.[1] In addition the field dependence of $R_H(H)$ has not been measured for temperatures above 36 K. Thus we are deprived of two pieces of experimental information. To continue the analysis to higher temperatures we need to introduce a fourth assumption: (d) the electron con-

centration n remains temperature independent from 36 to 58 K. This implies that the electron mobility μ_2 decreases with the same power law. The remaining four unknowns μ_1, ν_1, ν_2, and p are then computed from the measured ρ_1, ρ_2, $R_H(0)$, and μ_M. With this fourth assumption we find that (Fig. 1) the computed μ_1 (and ν_1) deviates only very slightly from its previous behavior; and p rises dramatically to four times its value at 36 K. The computed behavior of μ_1 provides justification for assumption (d) (that the electron pocket is not affected by the T_2 transition) while the exponential rise in p agrees with the gap analysis of Ref. 18. It is easy to see from the measured temperature behavior of $R_H/\rho_1\rho_2$ that, as the temperature approaches T_2 from below, either p rises rapidly or n decreases rapidly. Since the conductivity in both directions is also rising in this temperature range the first case is the obvious choice. (We have repeated the computation with the different assumption that p is held constant between 36 and 58 K and found that all the mobilities turn around and increase with temperature as T_2 is approached. This picture is certainly harder to justify.) Thus assumption (d) is the simplest one that provides physically reasonable behavior for the mobilities and carrier concentrations, under the four constraints provided by $R_H(0)$, ρ_1, ρ_2, and μ_M.

III. RESULTS AND DISCUSSION

Figure 1 shows the temperature dependence below T_2 of the four mobilities obtained by the solution of Eqs. (6)–(12). (For compactness the transverse hole mobility ν_c has been multiplied by 100.) All four mobilities show power-law behavior in this range before saturating at low temperatures. The longitudinal mobilities are surprisingly large at liquid-helium temperatures (270 000 cm^2/V sec). However, we note that at 40 K where the non-Ohmic effects are the most dramatic[18,19] μ_b and ν_b are only of the order of 3 000 cm^2/V sec. At 4 K the electron pocket anisotropy is 15 compared to 23.8 for the hole pocket. The carrier concentration n and p obtained from this analysis is shown in Fig. 2. As mentioned above both n and p are temperature independent below 40 K. Above 40 K, p rises rapidly, reflecting the thermal excitation of quasiparticles across a diminishing CDW gap on the hole surface. The solid line is the least-squares fit which provides the values of p used in all subsequent computations. The broken line indicates the assumed temperature-independent value of n above 40 K.

To check the validity of the solution we have made a least-squares fit to the calculated values in Fig. 1 and then used these values to recompute ρ_1, ρ_2, R_H, and μ_M. The electron concentration is taken to be fixed at 1.088×10^{18} cm^{-3} and p is taken from Fig. 2. Figure 3 shows the comparison of the computed ρ_1, ρ_2, and $R_H(0)$ with the experimental data while Fig. 4 shows the comparison for μ_M. The largest discrepancy occurs for $R_H(0)$, especially at temperatures below 12 K. This is to be expected for two reasons. Whereas ρ_1, ρ_2, and μ_M measure the additive effect of the two pockets the Hall constant measures the competition between the mobilities of the two pockets. Also R_H cannot be measured with the same precision as that of ρ_1 and ρ_2. At low temperatures where all

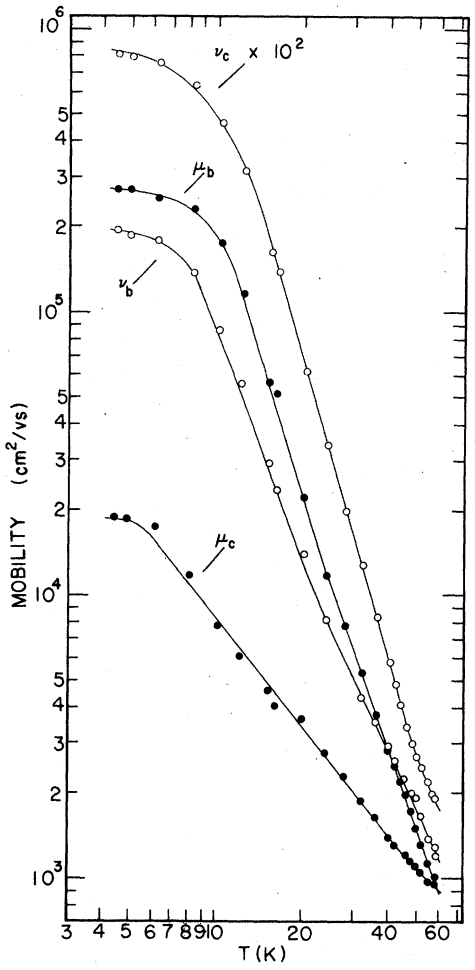

FIG. 1. Temperature dependence of the electron (solid circles) and hole (open circles) mobilities below 58 K. The data points are calculated from the experimental data using Eqs. (6)–(12). The lines are a least-squares fit to the data. In all cases the mobilities obey a power-law behavior except at low temperatures where they saturate. At 4 K the electron mobility ratio μ_b/μ_c equals 15, and the hole mobility ratio is 23.8. Note that the transverse hole mobility ν_c has been multiplied by 100.

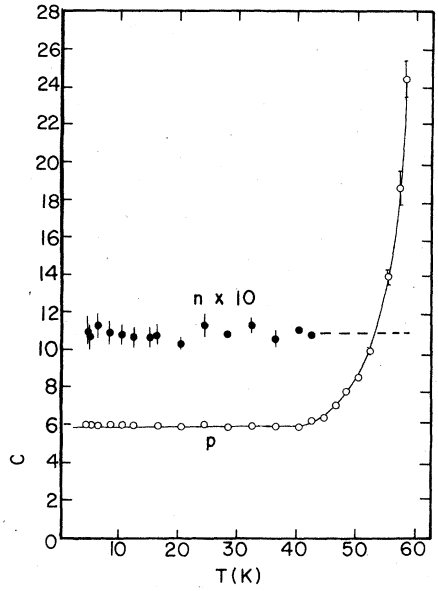

FIG. 2. Temperature dependence of the electron (solid circles) and hole (open circles) concentration. The data points below 40 K are computed from Eqs. (6)–(12) of text, and the error bars reflect the uncertainty in the measurements. Above 40 K the broken line indicates the assumed temperature-independent value of the electron concentration (1.09×10^{18} cm^{-3}). The open circles above 40 K are the computed values of p using this assumption. The solid line is the least-squares fit to the computed data on p.

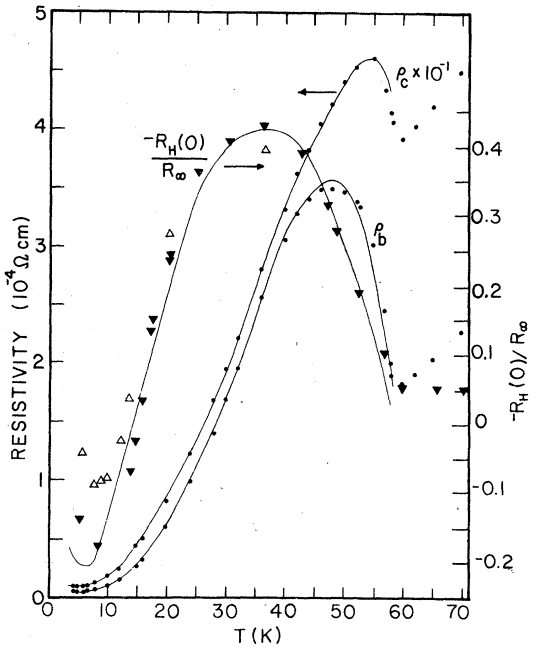

FIG. 3. Comparison of the experimental data for the resistivities ρ_b and ρ_c (circles), and the zero-field Hall constant $R_H(0)$ (triangles) with the two-band model calculation. The lines represent the values of $R_H(0)$, and ρ_b and ρ_c calculated using Eqs. (9) and (12). The values of the mobilities used are given by the full lines in Fig. 1. The electron concentration is assumed fixed at 1.09×10^{18} cm^{-3} and the hole concentration is given by the full line in Fig. 2. Values of $R_H(0)$ at low temperatures appear to be sample dependent. (The open and solid triangles are data from two samples normalized to the same value at infinite field.)

the mobilities are large R_H becomes very sensitive to the values of r, η, and ξ. At the same time, the zero-field value of R_H cannot be measured accurately due to the narrow range of fields over which R_H is field independent. Thus the computed values of r, η, and ξ below 12 K are accurate to only 20%. We have found also that the values of $R_H(0)$ and R^∞ at 2 K have a slight variation from sample to sample.[20]

The computed field dependence of R_H is shown in Figs. 5 (low fields) and 6 (high fields). (The experimental data in Fig. 6 are from FPC.) While the agreement in Fig. 5 is excellent except at very low temperatures, in Fig. 6 we have had to adjust the temperature of the sample to improve the fit at high fields. At low fields (~20 kG) the disagreement is larger. The value of $R_H(0)$ (the slope in Fig. 6) at 30 K is approximately equal and opposite in sign to R^∞ at 4.2 K in FPC's data whereas in the data used for this analysis the same quantity is only 40%. This accounts for the large discrepancy in Fig. 6 at low fields. The disagreement may be sample dependent.

We now turn to the SdH data and see to what extent the model described here is supported by the FS mapping obtained by means of the Shubnikov oscillations. The most extensive measurements on $NbSe_3$ are those of MB whose measurements indicate the presence of two branches and possibly a third. Along directions of the magnetic field where the oscillations are strong the data of MB agree with the preliminary data of M and FPC. The first branch which is the most well defined in MB's data corresponds to an approximately ellipsoidal surface with its principal axes along a^*, b, and c. The shortest dimension is along b and the longest is along c. If the semiaxis dimensions are k_{a^*}, k_b, and k_c the volume of the ellipsoid is $V=\frac{1}{3}S_c\times(S_a/4\pi\epsilon)^{1/2}$ where $S_a=4\pi k_b k_c$, $S_c=4\pi k_{a^*}k_b$, and $\epsilon=k_b/k_c$. From the SdH data of M, FPC, and MB, $S_c=0.3$ MG (2.86×10^{13} cm^{-2}), $S_a=1.05$ MG (1.00×10^{14} cm^{-2}). The carrier density within this FS pocket is thus equal to $n=2.17\times10^{17}/\sqrt{\epsilon}$ cm^{-3}. FPC find that $\epsilon\simeq\frac{1}{8}$ gives the best fit to the angular dependence of the frequency as the magnetic field is rotated towards the b axis. MB's data favor a smaller ϵ. In any case the carrier concentration is of the order of 6×10^{17}cm^{-3} which is in order-

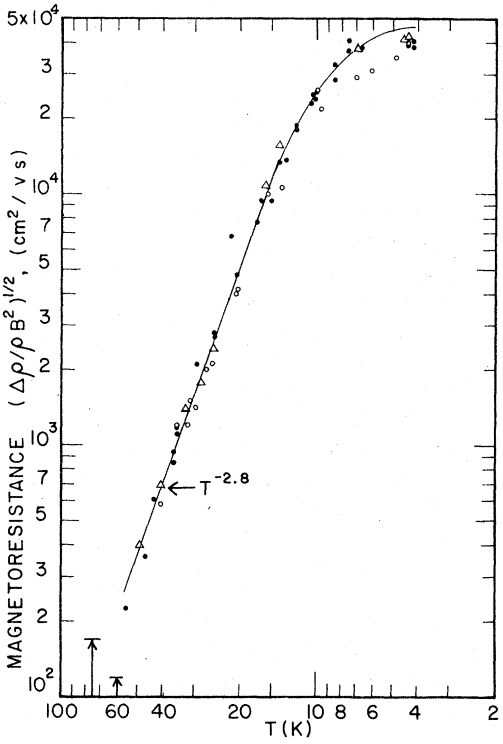

FIG. 4. Comparison of the experimental data for the magnetoresistance mobility with the two-band model calculation. The full line is calculated from Eq. (11) with the model parameters given by the full lines in Figs. 1 and 2. Data from three samples (Ref. 1) are displayed.

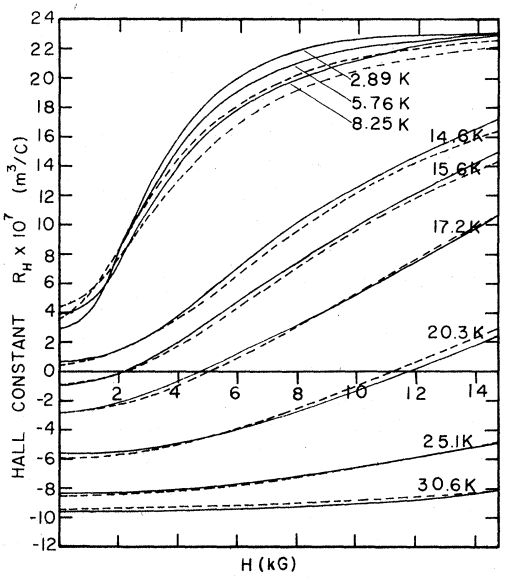

FIG. 5. Field dependence below 14 kG of the Hall constant at various temperatures below 40 K. The full lines are the experimental curves from Ref. 6 and the broken lines are calculated from Eqs. (6)–(8) using model parameters given by the full lines in Figs. 1 and 2. The computed R_H has been adjusted by a scale factor for comparison with the measurements (see Ref. 20). Agreement is excellent except at low temperatures where R_H is very sensitive to model parameters.

of-magnitude agreement with the electron concentration computed here (1.09×10^{18} cm^{-3}). Hence the ellipsoidal surface measured in the SdH data is probably the electron pocket. However, there are several difficulties in a careful comparison of the detailed SdH measurements of MB and FPC with our conclusions. First, the value of $\frac{1}{8}$ for ϵ would imply a mobility ratio of 64 (assuming a parabolic band) in the electron pocket. This is four times larger than the computed anisotropy in Fig. 1. This disagreement is probably due to the fact that this FS pocket resembles more a briefcase than an ellipsoid. MB's data agree with a cylindrical trajectory ($\epsilon \simeq 0$) with the magnetic filed tilted up to an angle of 70° from the a^*c plane.

Secondly, MB's data show other branches of the same order of magnitude in frequency which merge abruptly with the main branch. Over a certain angular range when the magnetic field is in the a^*c plane the main branch fades dramatically, leaving a ghost image of its original sec θ trajectory, while continuing with undiminished intensity into the new branch. These complications suggest that a simply connected ellipsoidal pocket is prob-

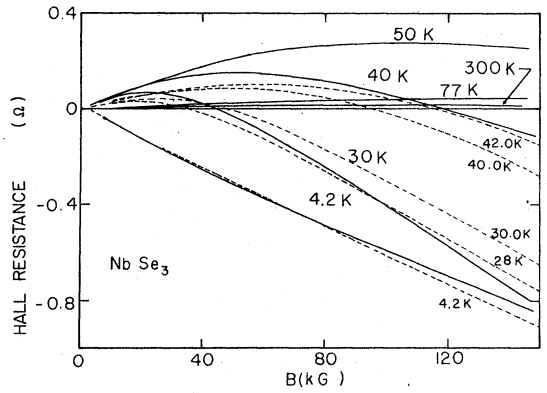

FIG. 6. Field dependence at high fields of the Hall resistance at various temperatures. The full lines are from Fleming, Polo, and Coleman (Ref. 8). The broken lines are calculated from the two-band model using parameters given by the solid lines in Figs. 1 and 2. The calculated Hall resistance has been normalized to agree with the experimental data at 4.2 K. The temperature of the sample has also been adjusted to give a better fit at high fields. There is a disagreement in the measured Hall polarity between Ref. 6 and Fleming *et al*. However, for the purpose of comparison we have changed the sign of the carriers in this figure.

ably too naive a picture. A possible explanation of these intriguing patterns is the intersection of the original pocket by higher-order superlattice Bragg planes. Indeed it may be shown[21] that several second-order images of the T_2-CDW Bragg plane oriented at 45° to the b-axis intersect the center of the Brillouin zone where the electron pocket would presumably be located. The faint ghost spots may be the result of magnetic breakdown[22] across these small gaps in analogy with the case[23] in Cr, while the abrupt appearance of a new branch may be the deflection of the electron trajectory into a new external orbit by the second-order gap.

The separation of the contributions of the two bands to the transport properties enables us to justify the argument used in the preceding paper with respect to $R_H(\rho_b\rho_c)^{-1}$. There it was argued that the quantity $A \equiv R_H(0)/(\rho_b\rho_c)$ had a temperature dependence which was dominated by the lifetime of the carriers. Dividing out the power-law behavior of the lifetimes enables us to observe the relative change in carrier concentration. From Fig. 1 the temperature dependence of the mobilities above 20 K is $T^{-1.2}(\mu_1)$, $T^{-2.8}(\mu_2)$, $T^{-3.5}(\nu_1)$, and $T^{-2.0}(\nu_2)$. Thus the quantity $A(T) = -(n\mu_1\mu_2 - p\nu_1\nu_2)$ has the temperature dependence $-(nT^{-4.0} - cpT^{-5.5})$ where c is a constant. Within the calculated parameters of the model the second term is 21% of the first at 50 K and increases to 61% at 58 K. Thus the first term dominates the behavior of A in this temperature range. We would then expect the quantity

$$A(T/T_1)^{3.875} \propto T^{-0.1}(n - cpT^{-1.4}),$$

to measure the relative change in carrier concentrations. The residual power law dependence $T^{-1.4}$ multiplying p unfortunately distorts the actual temperature dependence of p. However this is not serious near the transition because of the exponential increase in p. (A comparison of the data in Fig. 3 of the preceding paper with that in Fig. 2 here shows the slight difference between the temperature behavior of $A(T/T_1)^{3.875}$ and p.)

IV. CONCLUSION

The galvanomagnetic, conductivity and Shubnikov data obtained to date on $NbSe_3$ provide a rather complete picture of the low-temperature phase. To sort out the different components which contribute to the observed quantities we have adopted the simplest two-band model and used the experimental data to calculate the six unknowns in the model. Enough parameters are fixed by the measurements to leave no free parameters below 40 K. Above 40 K we have had to assume that the electron concentration remains temperature independent and shown that this is borne out self-consistently by the results. The picture that we obtain is that just below T_2 a CDW gap occurs on the hole surface. As the hole carriers are frozen out across the developing CDW gap, the total hole concentration decreases by a factor of 4. This results in only a factor of 2 rise in the longitudinal resistivity and an even smaller increase in the transverse resistivity because the electron mobilities are higher at this temperature. Below 40 K the carrier freeze out is complete, leaving 6.0×10^{18} cm^{-3} holes and 1.09×10^{18} cm^{-3} electrons. The remaining holes are from portions of the same FS which are not destroyed by the gap or may possibly belong to an entirely separate pocket. Below 36 K the Hall constant at zero field increases to more positive values and changes sign at 15 K because of the rapidly increasing hole mobilities. At very low temperatures the longitudinal mobilities become so large (~250 000 cm^2/V sec) that the Hall signal is rapidly driven to its infinite field value with the relatively modest field of 10 kG. In contrast to the Hall and resistivity data which show peak structures the transverse magnetoresistance obeys a smooth power-law behavior. This model also accounts for the strong field dependence of R_H (Fig. 6). The presence of the electron pocket is strongly indicated by the SdH data although the possibility of superlattice Bragg planes intersecting the electron FS may complicate the full interpretation of the SdH data. Evidence for the hole pocket is not apparent in the SdH data. Based on the parameters of this model, the resistivities, Hall constant, and magnetoresistance are calculated and good agreement is obtained with the experimental data.

The number of carriers participating in the T_2 transition is approximately 2×10^{19} cm^{-3} (16 times the electron concentration). This number, based on Fig. 2 is not meaningful if the gapping portion of the hole surface is not closed [since Eq. (5) is then no longer valid]. In fact the value of the transverse components of the spanning vector at T_2 $(0.5a^*, 0.5c^*)$[24] suggests that the FS that nests may be a cosine band[25] which intersects the Brillouin zone face. In this case Eq. (5) is clearly inadequate to describe contributions from all three sources. A third matrix obtained from a current term such as

$$\vec{J}_3 \cong \frac{2}{(e^{\beta\Delta}+1)} \frac{2e^2\tau}{(2\pi)^3} \int_{\text{gap}} \frac{dS_F}{|\hbar\vec{v}_{\vec{k}}|} \vec{v}_{\vec{k}} \cdot \vec{A}\vec{v}_{\vec{k}}$$

(where the integral is over the gapped portion of the FS) should be included. In spite of this qualification it is remarkable that the temperature dependence of p computed from Eq. (5) shows explicitly the exponential rise in quasiparticles as the

T_2 transition is approached. The number 2×10^{19} cm^{-3} should serve adequately as an order-of-magnitude estimate of the FS destroyed by the gap at T_2.

ACKNOWLEDGMENT

A useful discussion with Leo Falicov is gratefully acknowledged. This work was supported by the Office of Naval Research Contract No. N00014-77-C-0473. We wish to thank P. Monceau for sending a preliminary version of Ref. 9 prior to publication.

APPENDIX

Equations (6) and (9)–(12) may be reduced to a single equation involving only r as the unknown as follows. First, five of the equations are rewritten in terms of the dimensionless parameters [see Eq. (15)] r, ξ, and η, as

$$1/\rho_1 = p\nu_1(r\eta+1)\,,\quad 1/\rho_2 = p\nu_2(r\xi+1)\,,\quad R^\infty = 1/p(1-r)\,, \tag{A1}$$

$$\mu_M/(\rho_1\rho_2)^{1/2} = p\nu_1\nu_2\sqrt{r\eta}(\xi+1)\,, \tag{A2}$$

$$(R^\infty - R_0)/\rho_1\rho_2 = [rp\nu_1\nu_2/(1-r)](\xi+1)(\eta+1)\,. \tag{A3}$$

By forming the dimensionless constants C_1 and C_2 we eliminate p, ν_1, and ν_2. Thus we have

$$C_1 \equiv \frac{\mu_M(\rho_1\rho_2)^{1/2}}{(R^\infty - R_0)} = \frac{(1-r)}{\sqrt{r}}\,\frac{\sqrt{\eta}}{(1+\eta)}\,, \tag{A4}$$

$$C_2 \equiv \frac{\mu_M(\rho_1\rho_2)^{1/2}}{R^\infty} = \frac{\sqrt{r\eta}(1-r)(\xi+1)}{(r\xi+1)(r\eta+1)}\,. \tag{A5}$$

With r as the independent variable η and ξ can be expressed in terms of r through Eqs. (A4) and (A5). The mobilities ν_1 and ν_2 can then be found from Eq. (A1) in terms of r. Finally $R_H(H)/R^\infty$ can be computed as a function of H by Eq. (6) with r as an adjustable parameter. The value of r which provides the best fit of R_H/R^∞ to the experimental data (Fig. 5) is taken to be the correct solution.

[1]See references in preceding paper, N. P. Ong and J. W. Brill, Phys. Rev. B 18, 5265 (1978).

[2]See, for example, M. L. Boriack and A. W. Overhauser, Phys. Rev. B 16, 5206 (1977); D. Allender, J. W. Bray, and J. Bardeen, Phys. Rev. B 9, 119 (1974).

[3]N. P. Ong, J. W. Brill, J. Eckert, and J. Savage, S. K. Khanna, and R. B. Somoano (unpublished).

[4]R. R. Chianelli and M. B. Dines, Inorg. Chem. 14, 2417 (1975).

[5]D. W. Murphy, F. A. Trumbore, and J. N. Carides, J. Electro-Chem. Soc. 124, 325 (1977).

[6]N. P. Ong and P. Monceau, Solid State Commun. 26, 487 (1978). The c axis is mislabeled as the a axis in this reference.

[7]P. Monceau, Solid State Commun. 24, 331 (1977).

[8]R. M. Fleming, J. A. Polo, and R. V. Coleman, Phys. Rev. B 17, 1634 (1978).

[9]P. Monceau and A. Briggs, J. Phys. C 11, L465 (1978).

[10]S. K. Chan and V. Heine, J. Phys. F 3, 795 (1973).

[11]M. J. Rice and S. Strässler, Solid State Commun. 13, 125 (1973).

[12]J. Zittartz, Phys. Rev. 164, 575 (1967); 165, 605 (1968).

[13]See, for example, *The Fermi Surface*, edited by W. A. Harrison and M. B. Webb (Wiley, New York, 1962).

[14]See, for example, J. M. Ziman, *Principles of the Theory of Solids*, (Cambridge University, Cambridge, England, 1964), Chap. 7.

[15]See, for example, A. H. Wilson, *The Theory of Metals*, 2nd ed. (Cambridge University, Cambridge, England, 1965), p. 208.

[16]B. Abeles and S. Meiboom, Phys. Rev. 101, 544 (1956).

[17]H. C. Montgomery, J. Appl. Phys. 42, 2971 (1971).

[18]N. P. Ong, Phys. Rev. B 17, 3243 (1978).

[19]N. P. Ong and P. Monceau, Phys. Rev. B 16, 3443 (1977).

[20]Measurements of R^∞ on three samples give 2.37×10^{-6}, 1.41×10^{-6}, and 1.28×10^{-6} m^3/C. The values of n, p and the mobilities reported here as well as the data on the anisotropy apply to the third sample. In Fig. 5 the computed Hall constant has been multiplied by a scale factor of 1.85 to compare with the previously published measurements on sample 1 (Ref. 6).

[21]N. P. Ong (unpublished).

[22]L. M. Falicov, A. B. Pippard, and P. R. Sievert, Phys. Rev. 151, 498 (1966).

[23]L. M. Falicov and M. J. Zuckermann, Phys. Rev. 160, 372 (1967).

[24]R. M. Fleming, D. E. Moncton, and D. B. McWhan, Bull. Am. Phys. Soc. 23, 425 (1978).

[25]B. Horovitz, H. Gutfreund, and M. Weger, Phys. Rev. B 12, 3174 (1975).